J. Fluid Mech. (1967), *vol.* 30, *part* 2, *pp.* 371–384
Printed in Great Britain

Interferometric measurement of temperature gradient reversal in a layer of convecting air

By JOHN GILLE
Department of Meteorology, Florida State University, Tallahassee

(Received 31 March 1967)

Experiments in which a horizontal layer of convecting air is probed by one beam of a Michelson interferometer are described. When the localized interference fringes are horizontal, they indicate that the beam is wide enough to provide a suitable horizontal average. When the fringes are oriented nearly vertically, quantitative temperature measurements may be made. Results are presented for ratios (λ) of Rayleigh number to critical Rayleigh number of 1·48, 3·81 and 16·0. The temperature profile becomes more distorted from linear as the Rayleigh number is increased. An isothermal central region and thermal boundary regions each occupy one-third of the layer at $\lambda = 3{\cdot}81$. By $\lambda = 16{\cdot}0$ each boundary region occupies only one-quarter of the layer thickness, and the central region shows a reversed gradient. No full calculation is presently available to compare to the measurements. However, the shape assumption, using the first eigenfunctions of the linear stability problem, predicts the profile rather well for $\lambda = 1{\cdot}48$ and 3·81 if Nusselt number agreement is imposed.

1. Introduction

Recent work on finite amplitude convection, reviewed by Segel (1966) and Roberts (1966), aims at calculating the fields of velocity and temperature when the Rayleigh number exceeds the critical Rayleigh number by a finite amount. Predicted quantities subject to experimental test are the heat flux through the layer, the velocity in a plane, motion form and scale, and temperature distribution. Numerous heat flux measurements have been made (e.g. Malkus 1954*a*; Silverston 1958) but they are not a sensitive way to explore the internal state of the convecting fluid. Velocity measurements pose experimental problems. Motion form and size are usually assumed, rather than derived.

Measurements of temperature distribution are a more convenient and exacting manner of probing the fluid layer. Thomas & Townsend (1957), Deardorff & Willis (1966) and Somerscales & Dropkin (1966) have made such measurements with probes in the fluid. The probes must affect temperature and velocity in a manner difficult to calculate, however.

This paper describes the results of measuring the temperature field in a convecting layer of air by the interferometric method used by Gille & Goody (1964) (hereafter referred to as I) in studying stable temperature profiles distorted by

radiative heat transport. The interferometric method has the advantages of introducing no physical probes into the fluid, and giving a nearly instantaneous picture of the horizontally averaged vertical temperature distribution.

2. Experimental details

The convection cell has been described in I and in greater detail by Gille (1964) (hereafter referred to as II). Briefly, it consisted of a horizontal layer of air bounded above and below by flat circular aluminium plates, 25·34 cm in diameter. The plates were maintained at different temperatures, and held apart by spacers which set the thickness of the air layer. Layer thicknesses of 2 cm (actually 1·987) or 3·1 cm (actually 3·099) were employed in this investigation. The plates,

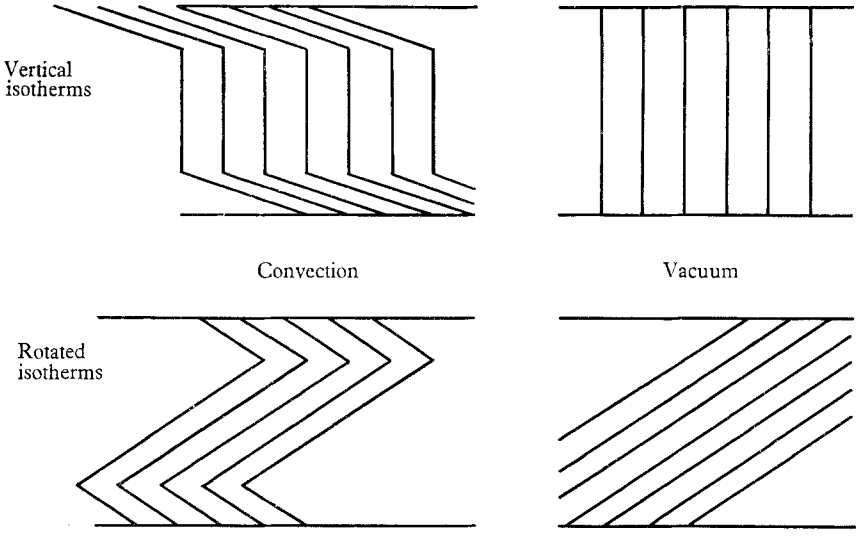

FIGURE 1. Schematic illustration of the effect of rotating the fringes optically.

with insulating disks and brass plates through which temperature controlled water was passed, were assembled in a vacuum tight aluminium vessel. Temperatures in the plates could be measured with thermocouples. By measuring temperature differences across the insulating disks, the heat flux could be determined.

The interferometer has also been described in I and II. It was of standard Michelson design, with one optical arm passing through windows and the air layer, while the other (reference) arm was outside the pressure vessel. A weighted wire hung in the reference arm to provide a vertical fiducial mark. When the air layer is isothermal, wedge fringes may be formed. If a vertical temperature difference is now imposed, at any level the fringes will be displaced relative to the centre by an amount proportional to the temperature difference between this level and the centre. The isothermal layer gives fringes characteristic of the optical system, which are identical to those obtained by evacuating the pressure vessel.

The optical characteristics may be altered for convenience. In particular, since we expect a vigorously convecting fluid to have a nearly isothermal central region and large gradients concentrated in the boundaries, we may rotate the

isothermal state through a large angle to better display behaviour in the boundary region. This is illustrated schematically in figure 1.

Experimental values of the Rayleigh number R were chosen for this investigation to give one case slightly above the critical Rayleigh number R_c, one several times as large, and another as high as the apparatus could reasonably go. The latter was limited by the size of the optics, the fact that the vessel could not be overpressured, and the desire to keep the local Rayleigh number fairly constant over the layer. With the temperature difference (top minus bottom) $\equiv \Delta\theta = -10°$, R varies by 13 % from top to bottom.

Run	C/S†	h (cm)	$\Delta\theta$ (°C)	R	$\frac{R}{1{,}786}$
1	C	1·987	−3·32	2,640	1·48
2	S	—	3·42	—	—
3	C	—	−8·71	6,800	3·81
4	C	3·099	−9·51	28,500	16·0
5	S	—	10·49	—	—

† C = unstable gradient; gas convecting.
S = stable gradient.

TABLE 1. Experimental conditions

The experimental situations finally analysed are listed in table 1. The positive $\Delta\theta$'s in the fourth column were stable cases, used to find the effective central optical length l_0 (see below). The data in I were used to calculate values of R in column 5. The last column shows R divided by R_c determined for air with this apparatus, 1786, (I). This is higher than the theoretical value 1708, but confirmed by recent measurements of Thompson & Sogin (1966).

An experimental run consisted of bringing the air into steady convection for several hours, making three photographs (0·6 full size) of the fringes on glass plates, evacuating the system and photographing the vacuum fringe system three times. Temperatures and pressures were read before and after each series of photographs.

As in I, the space on the photographs between the boundaries was divided by 21 equally spaced lines labelled $j = 0, \pm 1, \ldots \pm 10$, the latter two corresponding to the upper and lower boundaries respectively. Traces of the microphotometer scans along these lines were compared to the $j = 1$ trace to give means and standard deviations of the fringe positions. When the vacuum fringe positions are subtracted from the convection fringes, the fringe shift $N_j - N_1$ due to the fluid temperature distribution is obtained. On the traces, 1 mm corresponded to 0·01 fringe, or about 0·0125 °C.

We define a mean fringe shift antisymmetric about the centre as

$$\overline{N_j - N_0} = \tfrac{1}{2}\{(N_j - N_1) - (N_{-j} - N_1)\}. \tag{1}$$

By equation (39) in I,

$$\overline{N_j - N_0} = \frac{2(m_s - 1)\rho_0 l_0}{\lambda \rho_s}\left(\frac{1}{\rho}\frac{\partial \rho}{\partial \theta}\right)_0 (\theta_j - \theta_0), \tag{2}$$

where m is the index of refraction, ρ the density, λ the wavelength of the beam (5461 Å) and θ the temperature. Subscripts s, 0, j refer to conditions at STP, the centre of the layer, and the level j respectively. l_0 is the central length over which non-isothermal conditions are applied. All of these quantities are known or measured with the exception of l_0 and $(\theta_j - \theta_0)$, which is forced to be antisymmetric about the centre.

From thermocouple measurements we have $\Delta\theta = \theta_{10} - \theta_{-10} = 2(\theta_{10} - \theta_0)$ but because of boundary and refractive effects $N_{10} - N_0$ cannot be measured. For the stable case where the profile is determined by conduction, we can fit a straight line to $\overline{N_j - N_0}$, extrapolate to $\overline{N_{10} - N_0}$, and calculate l_0. For the convective profile we have no such means of extrapolating to the boundary; values of l_0 determined from conductive situations in the same geometry were used. Results can be checked through a knowledge of the Nusselt numbers.

We note that we could write

$$N_j - N_0 = K(j)\,(\theta_j - \theta_0),$$

where K may depend on j through l. Even though determinations of $N_j - N_0$ may be asymmetric, their relative variation shows how $\theta_j - \theta_0$ varies in time. This contains information about the relationship of variations at different levels which is lost in a series of measurements averaged over time at different levels. Information of this type will not be discussed here.

3. Representativeness of the measurements; horizontal fringes

The measurements represent an average over the width as well as the length of the sampling beam. They will be a suitable average if the beam width is larger than the scale of side-to-side variations. A special case occurs when there are no side-to-side variations; that is, the motion is two-dimensional in planes perpendicular to the boundary planes containing the beam direction.

Experimental (Koschmieder 1966) and theoretical (Schluter, Lortz & Busse 1965; Roberts 1966) studies lead us to expect the interferometer beam to traverse 12 or 8 round roll-cells at the two plate spacings, with a possible small effect due to the centre roll. Since Koschmieder's data only goes to $R = 5R_c$, the possibilities of three-dimensional motions at large $\lambda \equiv R/R_c$ cannot be ruled out.

The strongest evidence for representative averaging is obtained by orienting the vacuum fringes parallel to the bounding planes. With fluid in the layer, these fringes are isotherms. The spacing of the fringes depends inversely on the angle between the two reflecting surfaces, when vertical variations of optical path are included.

When central and boundary regions are well defined, the reference mirror can be adjusted to nearly compensate for the central region (central mode) or for the boundary region (boundary mode) as illustrated in figure 2. Fringe spacing provides a quantitative measure of temperature gradient, but is much less sensitive than the method discussed above. We shall only consider some qualitative characteristics of the horizontal fringe photographs.

Horizontal fringes for $\lambda = 1{\cdot}48$ are shown in figure 3*a*, plate 1, where the variation in planes parallel to the boundaries is seen to be small, as expected. Fringes

for $\lambda = 3{\cdot}6$ (central mode) are shown in figure 3*b*, plate 1, where some horizontal variation is seen. Sequential pictures showed time-dependent behaviour, with the formation and decay of buoyant regions in times of 20–30 s. It was later discovered that $\Delta\theta$ was changing slowly during this time. These may not be representative of the steady state.

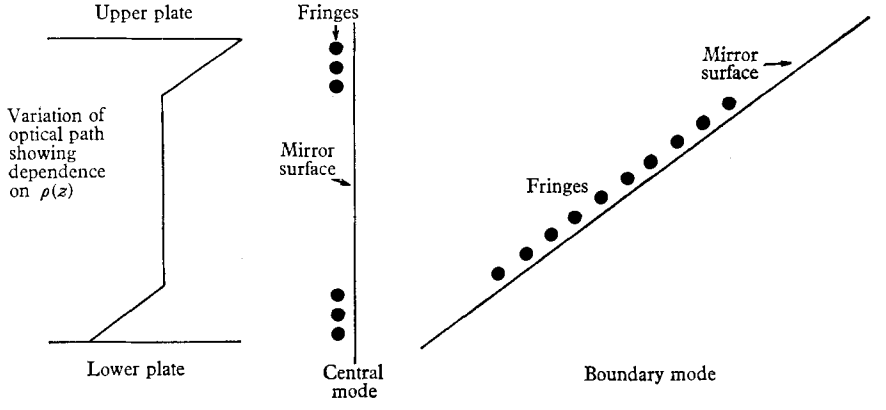

FIGURE 2. Schematic side view showing the formation of horizontal fringes.

Photographs in the central mode with $\lambda = 16{\cdot}0$ are shown in figures 3*c*, *d*, *e*, plate 1, where *d* follows *c* by 20 s and *e* follows *d* by 2 s. Horizontal and temporal variation is clearly shown, but the beam is wide enough to average approximately equal amounts of upward and downward fringe displacement, thereby constituting a reasonable average.

By contrast, figure 4, plate 2, shows the two photographs in the boundary mode at $\lambda = 16{\cdot}0$.

4. Quantitative measurements with perpendicular fringes

4.1. *The determination of* l_0

Photographs of the fringes for conduction with 2 cm spacers (run 2) are shown in figure 5, plate 2, where the right-hand fringes are the reference state, and the left-hand fringes show air heated above. Note that both sets of fringes are very nearly straight lines, and that the conduction fringes have their end-points rotated clockwise from the vacuum reference position.

By fitting a line of the form

$$\overline{N_j - N_0} = aj + bj^3$$

to the measurements from the photographs, b was shown to be statistically insignificant. The linear term immediately yields $\overline{N_{10} - N_0}$, which was inserted in (2) to obtain

$$l_0\,(2\text{ cm}) = 23{\cdot}76 \pm 0{\cdot}13\text{ cm}.$$

This is a considerable correction to the plate diameter of 23·34 cm, but in excellent agreement with the value $23{\cdot}86 \pm 0{\cdot}07$ cm obtained in I.

The same procedure yields

$$l_0\,(3{\cdot}1\text{ cm}) = 26{\cdot}10 \pm 0{\cdot}35\text{ cm}$$

for run 5. This is about 10 % greater than l_0 (2 cm), indicating that the larger plate separation and temperature difference lead to greater extension of the temperature field. The whole distance (26·06 cm) between the optical windows is now the effective working section.

4.2. *The convection fringes*

The convection and vacuum fringes for $\lambda = 1{\cdot}48$ are shown in figure 6*a*, plate 3. Here the convection fringes are curved, indicating that the fluid motions have distorted the temperature distribution. The end-points are also rotated in a counterclockwise direction, because the temperature gradient is in the opposite sense to that in figure 5. There is no well-formed boundary region, nor is the slope in the centre close to the slope of the vacuum reference state, showing that the centre is not isothermal at this low λ.

The interference fringes for $\lambda = 3{\cdot}81$ are shown in figure 6*b*, plate 3. Here a well-formed boundary layer is seen, with a central region whose slope is only slightly greater than the vacuum reference state. This implies a nearly isothermal central region. On one photograph there is an indication of a gradient reversal between $j = -1$ and $j = -3$. Calculations for free boundaries (e.g. Veronis 1966) predict this effect at about $\lambda = 4$.

The fringes for $\lambda = 16{\cdot}0$ in figure 6*c*, plate 3, show a further compression of the boundary layer. The slope of the centre region is less than in *b*, and on close inspection appears to be less than the slope of the vacuum fringes. Recalling figure 5, we note that this would mean an increase of temperature with height in the central portion of the layer.

4.3. *Quantitative results*

The photographs of vacuum fringes were all quite similar having standard deviations per point ranging from 0·01 fringe at the centre to nearly 0·02 fringe at the boundary. Agreement between photographs was excellent with no systematic differences. Weighted means have standard deviations ranging from 0·002 to 0·011 fringe. This is a measure of the resolution of the system, and includes the effects of inhomogeneities in the optical elements as well as fluctuations in open sections of the interferometer.

For convecting fringes, the standard deviations go from 0·01 fringe in the centre to maxima at the boundaries of 0·02, 0·035 and 0·05, respectively, at $\lambda = 1{\cdot}48$, 3·81 and 16·0.

The mean of the vacuum photographs was subtracted from the individual convective photographs to obtain 3 determinations of $\overline{N_j - N_0}$. Systematic differences between photographs occurred for all λ's, with spreads considerably larger than the standard deviations of the points. Maximum spreads between photos were (increasing λ) 0·10, 0·70 and 0·23. Whether the large variability for $\lambda = 3{\cdot}81$ is real or due to the sampling cannot be determined from the present data. These differences imply that the horizontal average is time dependent; i.e. that an

average with the present aspect ratios is not representative of an infinite spatial average. This is illustrated for $\lambda = 16{\cdot}0$ in figure 7.

The most interesting point at this λ is the backward bend in the central region of each photograph which confirms the small positive gradient suggested

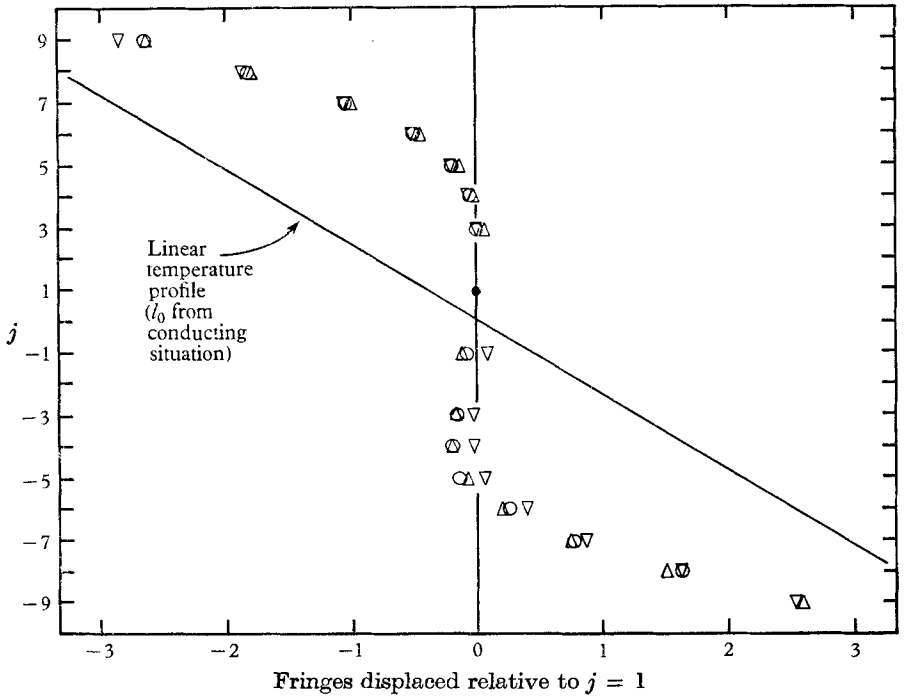

FIGURE 7. Fringe distortion relative to $j = 1$ for $\lambda = 16{\cdot}0$.
▽, photograph 1; △, photograph 2; ○, photograph 3.

	Points showing* reversal	Height of† reversal region	Region of‡ mean reversal
Photograph 1	1	$0{\cdot}15h$	$0{\cdot}35h$
2	5	$0{\cdot}35h$	$0{\cdot}45h$
2	4	$0{\cdot}25h$	$0{\cdot}45h$

* Points showing reversal are those more than 2σ to the reversal side of the axis.
† Reversal region is region with positive gradient between successive pairs of points.
‡ Region of mean reversal is region over which bottom temperature is warmer than top temperature.

TABLE 2. Summary of gradient reversal evidence

by figure 6*c*, plate 3, in spite of the overall large negative gradient. Data on this reversal is summarized in table 2. It should be emphasized that the indicated reversal is independent of l_0, and appears because the slope in the centre of the convecting fringes is less than the slope of the vacuum fringes. The gradient reversal is the most important result of this study, and is discussed further in §6.

To get a first determination of the horizontally averaged profile, a weighted mean of the values from the individual photographs was formed for each λ and made symmetric about $j = 0$. These were reduced to temperature differences with equation (2) and the appropriate value of l_0, and non-dimensionalized by $|\Delta\theta|$. The values obtained are given in table 3, as a function of dimensionless distance from the centre $\zeta = j/20$. The second column under $\lambda = 1{\cdot}48$ is explained in the next section.

	$\lambda = 1{\cdot}48$		3·81	16·0
ζ	$l_0 = 23{\cdot}76$	22·56	23·76	26·10
0·50	0·500	0·500	0·500	0·500
0·45	0·412 ± 0·005	0·433 ± 0·005	0·406 ± 0·004	0·317 ± 0·005
0·40			0·310 ± 0·003	0·208 ± 0·004
0·35	0·291 ± 0·004	0·307 ± 0·004	0·214 ± 0·002	0·111 ± 0·003
0·30			0·140 ± 0·002	0·041 ± 0·002
0·25	0·168 ± 0·004	0·177 ± 0·004	0·085 ± 0·002	0·005 ± 0·002
0·20			0·041 ± 0·002	−0·010 ± 0·001
0·15	0·087 ± 0·003	0·092 ± 0·003	0·018 ± 0·001	−0·010 ± 0·001
0·10				
0·05	0·025 ± 0·002	0·026 ± 0·002	0·002 ± 0·001	−0·005 ± 0·001
0	0·0	0·0	0·0	0·0

TABLE 3. $-\dfrac{\theta(\zeta) - \theta_0}{|\Delta\theta|}$

λ	β_{10}^*	Heat flux	de Graaf & van der Held† (1953)
1·48	1·77 ± 0·10	1·27 ± 0·12	1·34
3·81	1·88 ± 0·07	1·83 ± 0·17	1·95
16·0	3·67 ± 0·09	—	3·46

† Errors for experimental data are stated to be between 3 and 10%. These presumably lie in the region of larger errors, associated with small temperature differences at these relatively low values of λ.

TABLE 4. Interferometric and heat flux determinations of Nusselt number

5. Nusselt number determinations

The Nusselt number Nu is defined as the ratio of mean heat flux through the layer to the conductive heat flux down the mean temperature gradient. Since there are no motions at the boundary, the heat flux there is purely conductive. Denoting the boundary gradient by β_{10} and the mean gradient by $\bar{\beta} = \Delta\theta/h$,

$$Nu = \beta_{10}/\bar{\beta} = \beta_{10}^* \approx \frac{\theta_{10} - \theta_9}{0{\cdot}05h} \Big/ \frac{\Delta\theta}{h} = 20\frac{\theta_{10} - \theta_9}{\Delta\theta},$$

since the experimental and theoretical gradients all appear rather constant near the boundary, and we have no information on their variation. Using temperature values from table 3, we obtain the results in the second column of table 4.

Nu can also be measured directly with this apparatus in the manner described in I. Introduction of the copper inset for the optical windows has a measurable effect on the heat flux, however, and Nusselt numbers determined simultaneously with interferometric profiles are not as precisely determined as Nusselt numbers measured separately. These determinations are listed in the third column of table 4. Unfortunately, time limitations precluded some auxiliary measurements on the cell with the wider spacing, so simultaneous determinations for that case are not available.

The fourth column shows Nusselt numbers based on the empirical formula of de Graaf & van der Held (1953) based on their experimental data.

The interferometrically determined boundary gradients for $\lambda = 3{\cdot}41$ and $16{\cdot}0$ show satisfactory agreement with measured heat fluxes, in view of the errors, and suggest that the weighted mean profiles in table 3 are reasonably accurate descriptions of the mean state of the fluid. β^*_{10} for $\lambda = 1{\cdot}48$ is much larger than the heat flux values (underlining the problem outlined above: the lack of knowledge of temperature and fringe shifts at two locations simultaneously, or alternatively l_0). A change of l_0 by 5 % to $l'_0 = 22{\cdot}56$ cm is sufficient to convert the Nusselt number to agree with the values of de Graaf & van der Held. Non-dimensional temperatures calculated with l'_0 are shown in the second column under $\lambda = 1{\cdot}48$ in table 3.

6. Discussion of the results

The results for the three convective runs are plotted together in figure 8. As anticipated, with increasing λ the profile becomes progressively more distorted from the linear, conductive profile. Note that for $\lambda = 1{\cdot}48$, the change of l_0 from 23·76 cm (dashed line) to 22·56 (solid line) changes the boundary slope, as intended, but leads to small differences in the centre. By $\lambda = 3{\cdot}81$, a nearly isothermal central region occupies the central third of the layer while thermal boundary layers are confined to the outer thirds on either side. When $\lambda = 16{\cdot}0$, each boundary region occupies only one-quarter of the layer, and the central region displays a reversed gradient.

The occurrence of gradient reversal on every photograph for $\lambda = 16{\cdot}0$ indicates that the vertical temperature gradient averaged over an infinite horizontal area may well be reversed. The profile overshoots the centre by $1\frac{1}{2}$ % of $\Delta\theta$. Veronis (1966) predicts 6 % for free boundaries. This will occur when warm fluid is forced toward the lower plate by rising hot fluid, before it has come to temperature equilibrium with the upper boundary. Some of the fluid's kinetic energy is used to lower warm light fluid, and similarly to raise cold dense fluid, increasing the potential energy of the system.

This implies a positive correlation between the temperature of the driving elements and the driven elements, which would be present in any regular flow, whether of roll or polygonal form. The correlation would be expected to decrease as the motion becomes more disorganized and turbulent. Deardorff's (1965) calculations at $R = 6{\cdot}75 \times 10^5$ indicated a slight gradient reversal, but measurements at $1{\cdot}5 \times 10^6$ did not. Further measurements with a long resistance wire

reported by Deardorff & Willis (1966) at $R = 6{\cdot}3 \times 10^5$, $2{\cdot}5 \times 10^6$ and $1{\cdot}0 \times 10^7$ show no reversal. This may be due to the introduction of a conducting probe, but is very likely real since they have highly turbulent flows. Veronis (1966) also gives reasons for the temperature field associated with rolls to differ from that for a fully turbulent situation.

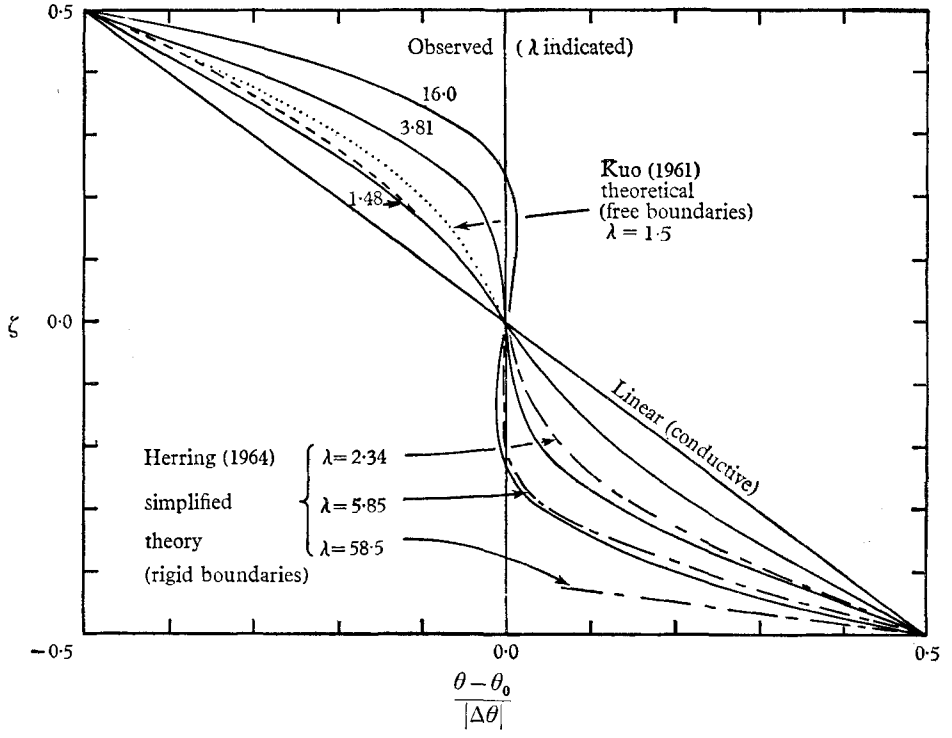

FIGURE 8. The observed mean temperature profiles (solid lines) plotted non-dimensionally with some theoretical predictions. For $\lambda = 1{\cdot}48$, the solid line is for $l_0 = 22{\cdot}56$ cm, the dashed line is for $l_0 = 23{\cdot}76$ cm.

Thomas & Townsend (1957) using a Wollaston wire probe, found a region of gradient reversal at $R = 6{\cdot}75 \times 10^5$, but ascribed it to large-scale circulation in the apparatus.

This result is also indicated by the refractive measurements of Schmidt & Saunders (1938), although they do not comment upon it. At $\lambda = 7$ in water (their figure 4*a*) there is no measurable gradient in the centre of the fluid, as they state. They apparently did not look for gradient reversal, nor is it clear whether their arrangement was sensitive enough to detect it. In their figures 4*d* and 4*e* (for water at $\lambda = 76$) some of the lines extend below the indicated centre of the layer, implying regions of reversed gradient. In fact, some images in 4*d* are below the lower boundary, *requiring* a reversed gradient.

Although the central gradient is adverse, the mean flux of heat is upward. The counter gradient fluxes disagree with the suggestion advanced by Malkus (1954*b*) that '. . .in the absence of mean forces other than those due to the temperature distribution itself this mean heat flux, H, can never be up the average

thermal gradient'. By discussing the local change of thermal variance, Deardorff (1966) has shown that such fluxes are possible, due to very buoyant elements which penetrate the stable region.

The experimental result has an immediate implication for the Malkus theory of turbulence (Malkus 1963; Spiegel 1964). In one form, this theory says that the state which will be observed in a convecting layer will be that one which maximizes the heat transport subject to constraints including the requirement that the mean gradient be everywhere non-positive. This particular constraint in its absolute form now appears in some doubt. However, this constraint is not regarded as fundamental to the theory by some (Howard 1963; R. S. Lindzen, private communication). The present result is certainly not a refutation of the Malkus theory.

7. Comparison with theoretical profiles

There are no published profiles for rigid boundaries which include the effects of higher spectral components. Kuo (1961), Veronis (1966) and Fromm (1965) have made detailed calculations for free boundaries which agree reasonably with each other. Kuo's curve for free boundaries at $\lambda = 1{\cdot}5$ in the upper part of figure 8 shows considerably greater profile distortion than that observed, as one might expect.

The approximate calculations of Herring (1964) for $\lambda = 2{\cdot}34$, $5{\cdot}85$ and $58{\cdot}5$ (boundary only) are shown in the lower part of figure 8. They agree reasonably well with the observations, although they are too distorted for large λ (Veronis 1966).

Roberts (1966) reviews the manner in which the shape assumption and power integrals may be used to compute the mean temperature profile near $\lambda = 1$. This may be written

$$\frac{\theta(\zeta)-\theta_0}{|\Delta\theta|} = -\zeta[1+\Gamma\lambda^{-1}(\lambda-1)]+\Gamma\lambda^{-1}(\lambda-1)F(\zeta),$$

where $\zeta = j/20$, $\Gamma = 1{\cdot}445$,

$$F(\zeta) = \int_0^{\zeta} T^c w^c d\zeta \Big/ \int_{-\frac{1}{2}}^{\frac{1}{2}} T^c w^c d\zeta$$

and T^c, w^c are eigenfunctions of the linear stability problem for temperature departure from the horizontal mean and vertical velocity. These functions are tabulated by Reid & Harris (1958).

Since Nu (theoretical) $= -(\partial\theta/\partial\zeta)_{\pm\frac{1}{2}} = 1+\Gamma\lambda^{-1}(\lambda-1)$ the deviation from the linear gradient may be written

$$\frac{\theta(\zeta)-\theta_0+\zeta|\Delta\theta|}{|\Delta\theta|} = -[Nu\,(\text{theoretical})-1][\zeta-F(\zeta)]. \tag{3}$$

These predicted distortions, shown as solid lines in figure 9, are larger than the experimental values. This technique also yields Nusselt numbers larger than observed, suggesting that we write

$$\frac{\theta(\zeta)-\theta_0+\zeta|\Delta\theta|}{|\Delta\theta|} = -[Nu\,(\text{observed})-1][\zeta-F(\zeta)]. \tag{4}$$

The dashed lines in figure 9 show these distortions, which agree well with observed values. The first eigenfunctions are able to predict the shape of the temperature deviation up to nearly four times the critical Rayleigh number, although the amplitude calculated from the power integrals is too large. The clear implication is that higher modes are excited and consume energy, but contribute

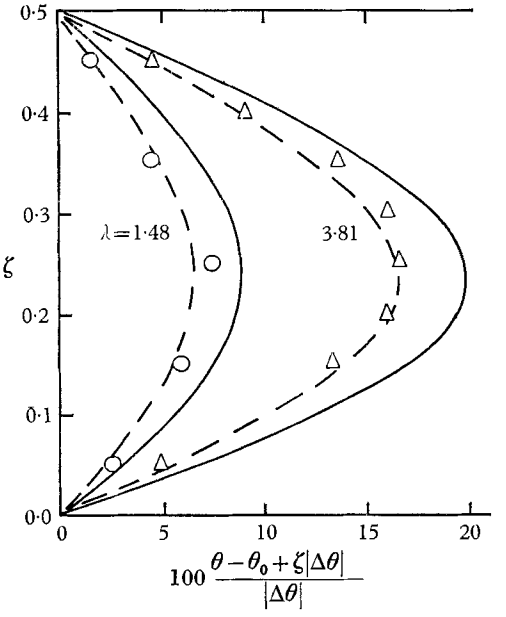

FIGURE 9. Profile distortion at $\lambda = 1{\cdot}48$ and $3{\cdot}81$. The full line is computed according to (3), the dashed line according to (4). The points are measured; ○, $\lambda = 1{\cdot}48$; △, $\lambda = 3{\cdot}81$. Standard deviations are less than the size of the symbols.

little to the heat flux and average temperature field. At $\lambda = 16{\cdot}0$ the solution involving a single eigenfunction is very much more distorted than the observations when boundary Nusselt numbers are matched. Higher modes are playing a large part at this λ.

Platzman (1965) and Roberts (1966) performed elaborate calculations which yielded profiles *more* distorted than the power integral calculations, in greater disagreement with the observations.

There are no other detailed measurements of temperature distribution for this range of Rayleigh numbers in air known to this writer. Measurements in liquids with probes appear to have large errors.

8. Conclusions

The most important result is the discovery of the region of reversed temperature gradient at high Rayleigh numbers, as predicted numerically. The reversal is consistent with the photos of Schmidt & Saunders (1938). An explanation has been offered for the failure of Deardorff & Willis (1966) to observe gradient reversal at much larger Rayleigh numbers. Further numerical work should be done to calculate profiles between rigid boundaries for λ's close to the experimental

ones. More experimental work would be desirable, to explore the characteristics of the temporal variation and λ dependence of the region of reversal.

The progressive distortion of the profile with λ is in agreement with intuitive understanding. The accuracy of the distortion predictions based on the first eigenfunctions should be viewed with caution, because the constraints impose considerable agreement. None the less, the eigenfunction predictions agree with observations considerably better than a parabola or sine function similarly constrained; they are too small at $\zeta = 0{\cdot}25$. The observations support the view that the first eigenfunction is predominant in establishing the temperature field, with higher modes having little effect other than siphoning energy from the dominant mode. Variability of the profiles in time indicates that an average through a distance equivalent to 4–6 wavelengths is not representative of an infinite array.

Finally, the power of the interferometric method of probing air layers has been amply illustrated. Not only have temperatures been measured with good accuracy, but information about horizontal variations across the beam, details of the isotherms in the centre or boundaries, and time variability of mean profiles can be extracted. Clearly, this method can provide a detailed view of the beguiling complexities of a fluid layer heated from below.

Supported in part by the Atmospheric Sciences Section, National Science Foundation, NSF Grant G24903 to Harvard University. Data reductions supported by NASA Grant NSG-173 to Florida State University. I am indebted to Professor Richard Goody for valuable suggestions and Professor Seymour Hess for encouragement.

REFERENCES

DEARDORFF, J. W. 1965 A numerical study of pseudo three-dimensional parallel plate convection. *J. Atmos. Sci.* **22**, 419–35.

DEARDORFF, J. W. 1966 The counter-gradient heat flux in the lower atmosphere and in the laboratory. *J. Atmos. Sci.* **23**, 503–6.

DEARDORFF, J. W. & WILLIS, G. E. 1966 Investigation of turbulent thermal convection between horizontal plates. National Center for Atmospheric Research, Boulder, Colorado. Prepublication review manuscript no. 140, 58 pp. available from authors.

FROMM, J. E. 1965 Numerical solutions of the nonlinear equations for a heated fluid layer. *Phys. Fluids*, **8**, 1757–69.

GILLE, J. C. 1964 Convective instability in a layer of radiating fluid. Ph.D. Thesis, Dept. of Geophysics (Course XII), M.I.T., Cambridge, Mass.

GILLE, J. C. & GOODY, R. M. 1964 Convection in a radiating gas. *J. Fluid Mech.* **20**, 47–79.

DE GRAAF, J. G. & VAN DER HELD, E. F. M. 1953 The relation between the heat transfer and the convection phenomena in enclosed plane layers. *Appl. Sci. Res.* A **3**, 393–409.

HERRING, J. R. 1964 Investigation of problems in thermal convection: Rigid Boundaries. *J. Atmos. Sci.* **21**, 277–90.

HOWARD, L. N. 1963 Heat transport by turbulent convection. *J. Fluid Mech.* **17**, 405–32.

KOSCHMIEDER, E. L. 1966 On convection on a uniformly heated plane. *Beitr. Phys. Atmos.* **39**, 1–11.

KUO, H. L. 1961 Solution of the non-linear equations of cellular convection and heat transport. *J. Fluid Mech.* **10**, 611–34.

MALKUS, W. V. R. 1954*a* Discrete transitions in turbulent convection. *Proc. Roy. Soc.* A**225**, 185–95.

MALKUS, W. V. R. 1954*b* The heat transport and spectrum of thermal turbulence. *Proc. Roy. Soc.* A**225**, 196–212.

MALKUS, M. V. R. 1963 Outline of a theory of turbulent convection. *Theory and Fundamental Research in Heat Transfer*, ed. by J. A. Clark. New York: MacMillan.

PLATZMAN, G. W. 1965 The spectral dynamics of laminar convection. *J. Fluid Mech.* **23**, 481–510.

REID, W. H. & HARRIS, D. L. 1958 Some further results on the Bénard problem. *Phys. Fluids*, **1**, 102–10.

ROBERTS, P. H. 1966 On non-linear Bénard convection. *Non-equilibrium Thermodynamics, Variational Techniques and Stability*, edited by R. J. Donnelly, R. Herman, and I. Prigogine. University of Chicago Press.

SCHLUTER, A., LORTZ, D. & BUSSE, F. 1965 On the stability of steady finite amplitude convection. *J. Fluid Mech.* **23**, 129–44.

SCHMIDT, R. J. & SAUNDERS, O. A. 1938 On the motion of a fluid heated from below. *Proc. Roy. Soc.* A**165**, 216–28.

SEGEL, L. A. 1966 Non-linear hydrodynamic stability theory and its applications to thermal convection and curved flows. *Non-equilibrium Thermodynamics, Variational Techniques and Stability*, edited by R. J. Donnelly, R. Herman and I. Prigogine. University of Chicago Press.

SILVESTON, P. L. 1958 Warmedurchgang in waagerechten Flussigheitsschichten. *Forsch. Geb. Ing. Wes.* **24**, 29–32, 59–69.

SOMERSCALES, E. F. C. & DROPKIN, D. 1966 Experimental investigation of the temperature distribution in a horizontal layer of fluid heated from below. *Int. J. Heat Mass Transfer* **9**, 1189–204.

SPIEGEL, E. A. 1964 On the Malkus theory of turbulence. *Mechanics of Turbulence*. New York: Gordon and Breach.

THOMAS, D. B. & TOWNSEND, A. A. 1957 Turbulent convection over a heated horizontal surface. *J. Fluid Mech.* **2**, 473–92.

THOMPSON, H. A. & SOGIN, H. H. 1966 Experiments on the onset of thermal convection in horizontal layers of gases. *J. Fluid Mech.* **24**, 451–79.

VERONIS, G. 1966 Large amplitude Bénard convection. *J. Fluid Mech.* **26**, 49–68.

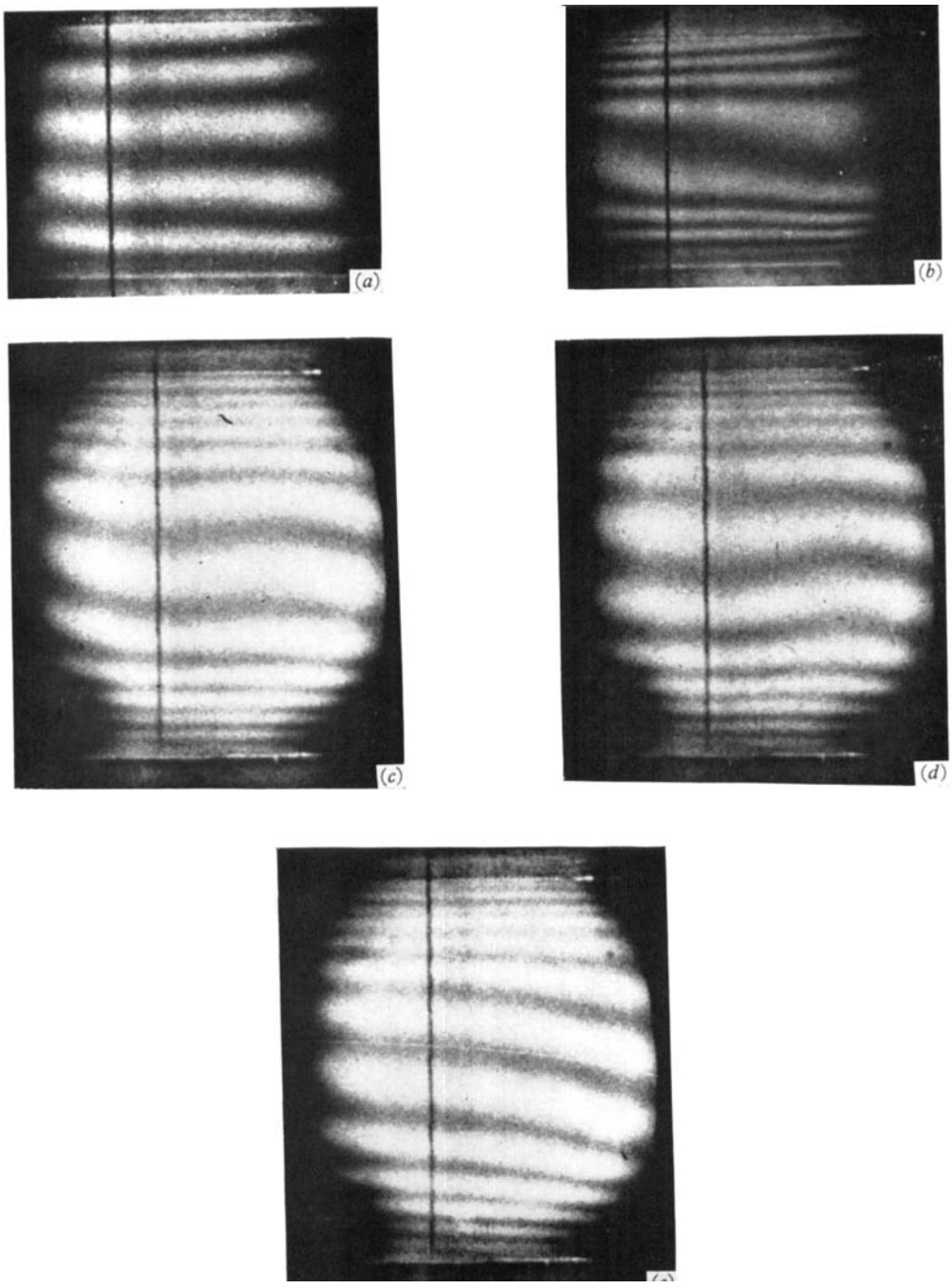

FIGURE 3. Horizontal fringes (central mode). (*a*) $\lambda = 1{\cdot}48$, (*b*) $\lambda = 3{\cdot}6$; (*c*) $\lambda = 16{\cdot}0$; (*d*) $\lambda = 16{\cdot}0$, 20 s after (*c*); (*e*) $\lambda = 16{\cdot}0$, 2 s after (*d*). Dark line is vertical fiducial mark.

(*Facing p.* 384)

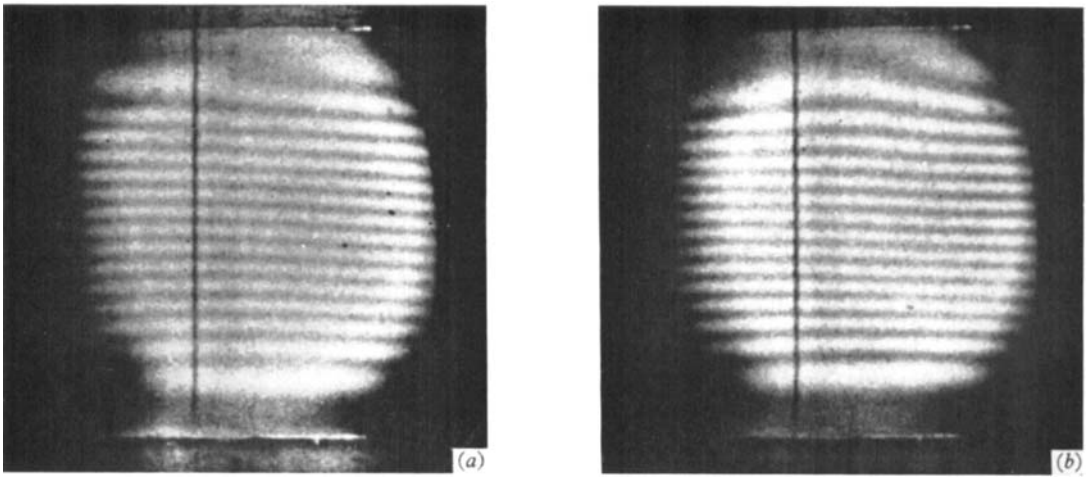

FIGURE 4. Horizontal fringes (boundary mode), $\lambda = 16{\cdot}0$. (*b*) 20 s after (*a*). A region of warm fluid can be seen reaching the upper plate.

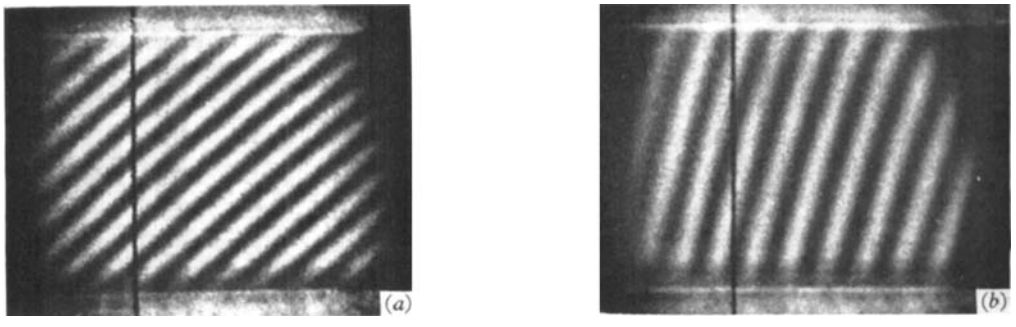

FIGURE 5. Interference fringes for run 2. Vacuum reference on right, air conducting on left. Fringes are rotated in clockwise sense.

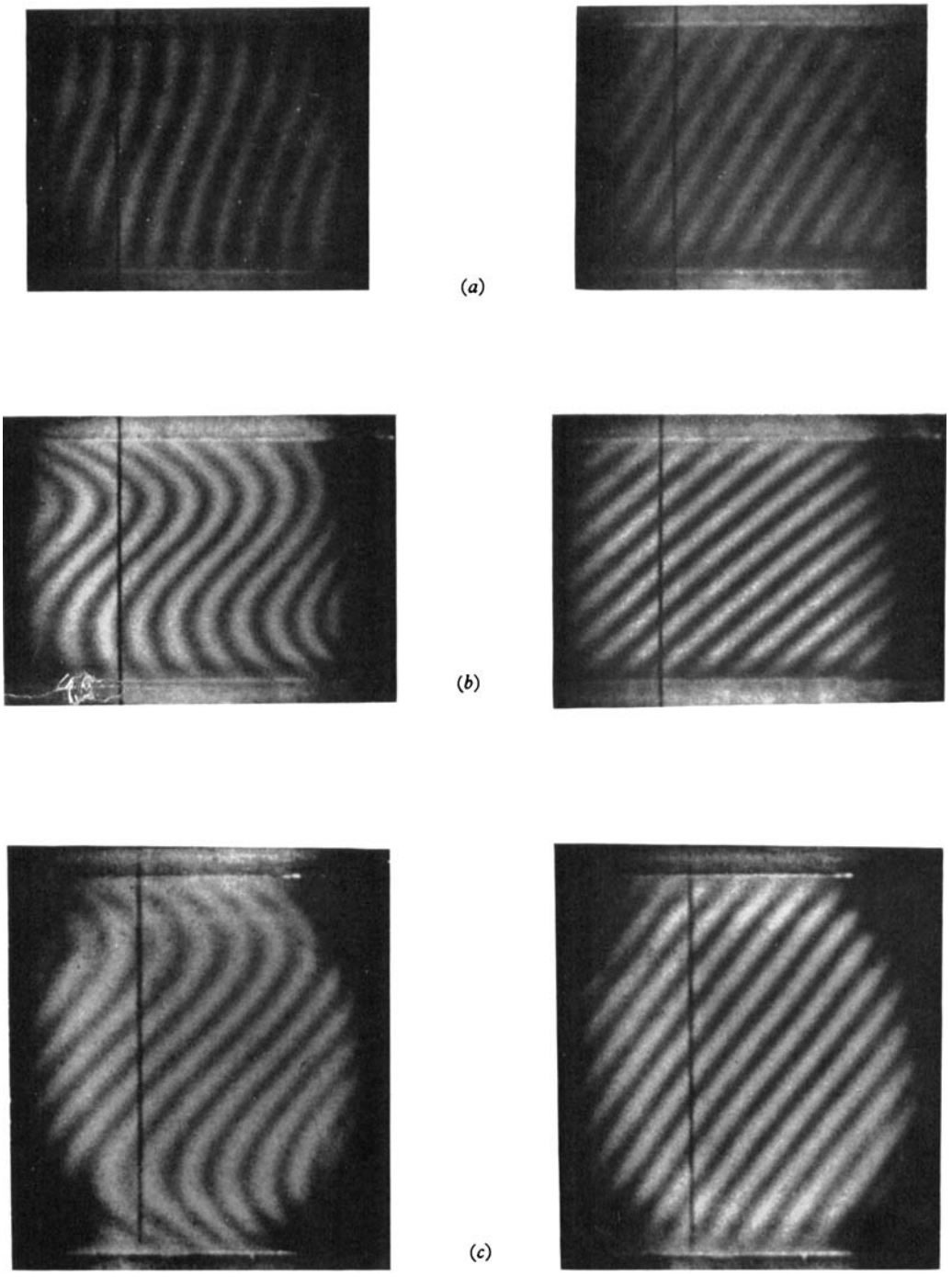

FIGURE 6. Interference fringes, showing distortion of temperature by fluid motion. Vacuum reference is on right, convecting air is on left. (*a*) $\lambda = 1{\cdot}48$; (*b*) $\lambda = 3{\cdot}81$; (*c*) $\lambda = 16{\cdot}0$. Fringes are rotated in counter-clockwise sense.